Influence of the sputtering flow regime on the structural properties and magnetic behavior of Fe-Ga thin films (Ga ∼ 30 at.%)

A. Muñoz-Noval,[1] A. Ordóñez-Fontes,[2] and R. Ranchal[2,*]

[1]*Department of Applied Chemistry, Hiroshima University, Higashi-hiroshima, Hiroshima 739-8527, Japan; BM25-SpLine, the Spanish Collaborating Research Group (CRG) at the European Synchrotron Radiation Facility (ESRF), Grenoble, France; and Instituto de Ciencia de Materiales de Madrid-Consejo Superior de Investigaciones Científicas (CSIC), Madrid, Spain*

[2]*Departamento de Física de Materiales, Facultad de Ciencias Físicas, Universidad Complutense de Madrid, Ciudad Universitaria s/n, Madrid 28040, Spain*

(Received 26 November 2015; revised manuscript received 14 April 2016; published 7 June 2016)

In this paper we analyze the structure of Fe-Ga layers with a Ga content of ∼30 at.% deposited by the sputtering technique under two different regimes. We also studied the correlation between the structure and magnetic behavior of the samples. Keeping the Ar pressure fixed, we modified the flow regime from ballistic to diffusive by increasing the distance between the target and the substrate. X-ray diffraction measurements have shown a lower structural quality when growing in the diffusive flow. We investigated the impact of the growth regime by means of x-ray absorption fine structure (XAFS) measurements and obtained signs of its influence on the local atomic order. Full multiple scattering and finite difference calculations based on XAFS measurements point to a more relevant presence of a disordered $A2$ phase and of orthorhombic Ga clusters on the Fe-Ga alloy deposited under a diffusive regime; however, in the ballistic sample, a higher presence of $D0_3/B2$ phases is evidenced. Structural characteristics, from local to long range, seem to determine the magnetic behavior of the layers. Whereas a clear in-plane magnetic anisotropy is observed in the film deposited under ballistic flow, the diffusive sample is magnetically isotropic. Therefore, our experimental results provide evidence of a correlation between flow regime and structural properties and its impact on the magnetic behavior of a rather unexplored compositional region of Fe-Ga compounds.

DOI: 10.1103/PhysRevB.93.214408

I. INTRODUCTION

In recent years, $Fe_{100-x}Ga_x$ alloys have received great attention due to their unique magnetoelastic properties [1–9]. For these compounds, the magnetostriction constant (λ_s) dependence with Ga proportion shows two peaks for Ga contents around 18 and 28 at.% [8]. The exact position of these peaks depends on the thermal history during processing, and higher magnetostriction values are achieved for quenched samples with Ga content of 19 and 30 at.% [8]. Also, it is known that the magnetic anisotropy of Fe-Ga alloys is closely related to magnetostriction. Starting from pure Fe, magnetic anisotropy decreases while the magnetostriction constant increases as Ga is introduced in the Fe matrix [10]. Therefore, the study of the magnetic anisotropy in these compounds appears to be crucial for the understanding and control of their magnetoelastic properties. Although knowledge of the properties of Fe-Ga alloys with compositions around the two peaks of magnetostriction seems to be of relevance, most papers have been devoted to the study of compounds around the first peak (Ga ∼19 at.%) in spite of the larger magnetostriction constant around the second peak (Ga ∼30 at.%). The first, and more studied, magnetostriction peak seems to be the result of the inclusion of disordered Ga substituting Fe randomly in the body-centered-cubic (bcc) lattice sites ($A2$ phase). The second high magnetostrictive state of the alloy is more complex. The $D0_3$ order appears beyond 19 at.% Ga [8], and, eventually, some papers point to the formation of Ga aggregates above 28 at.% Ga [11]. Thus, obtaining this second metastable state seems more difficult to achieve, and identification of the nature of Ga aggregates remains to be investigated.

Sputtering is a widely used technique to obtain thin films for both basic research and industrial applications. Although several papers deal with the growth of Fe-Ga thin films by sputtering [11–17], the impact of different phenomena occurring during sputtering deposition has not been completely clarified or quantified. For example, neutrals (atoms ejected from the target upon the impact of energetic particles) suffer collisions during their movement from target to substrate [18–20]. If the number of collisions is low, neutrals keep their momentum and energy until the substrate and the sputtering process takes place under ballistic flow [18]. However, neutrals lose their kinetic energy and momentum, reaching the substrate just with thermal energy if the number of collisions is large enough to produce their thermalization [21]. λ is the thermalization mean free path. When λ is greater than the distance between target and substrate (L), deposition takes place under ballistic flow. When λ is less than L, neutrals arrive thermalized at the substrate. In this last case, neutrals can move from the point at which they are thermalized (λ) to the position of the substrate (L) because of the composition gradient existing between λ and L [21].

All these interactions between neutrals and plasma are expected to have an impact on the structural properties of the samples and, hence, on their magnetic behavior. In this paper, we present a detailed investigation on the effect of the flow regime on the local and long-range structure of Fe-Ga compounds with a Ga content around 30 at.%. Our results show that the structural differences have an effect on the in-plane magnetic anisotropy ($K_{\text{in-plane}}$) developed in layers grown under different regimes.

*Corresponding author: rociran@ucm.es

II. EXPERIMENTAL DETAILS

Samples were grown by the DC magnetron sputtering technique at room temperature on glass substrates. Deposition was carried out in oblique incidence, with an angle between the vapor beam and the perpendicular to the sample of about 25°. The 200-nm-thick Fe-Ga films were deposited from a target with a composition of $Fe_{72}Ga_{28}$. We used an Ar pressure of 0.3 Pa and a growth power of 50 W in all cases. The distance between target and substrate was 9 and 14 cm, and as discussed below, these two distances correspond to the ballistic and diffusive regimes, respectively. We used 30-nm Mo layers as buffers and capping. Mo was also deposited by DC sputtering with a power of 90 W and in an Ar pressure of 0.3 Pa.

X-ray diffractometry (XRD) in the Bragg–Brentano configuration was performed in a Philips X'Pert multipurpose diffractometer (MPD) using the CuK_α wavelength (1.54056 Å). The composition of the samples was analyzed by means of energy-dispersive x-ray spectroscopy (EDS) with a Leica 440 scanning electron microscope (SEM) operated at 8 kV and 1.5 nA. The in-plane hysteresis loops were measured at room temperature in a vibrating sample magnetometer (VSM) from Lake Shore.

The x-ray absorption fine structure (XAFS) measurements were performed at the Fe K edge (7112 eV) and the Ga K edge (10 367 eV) in fluorescence yield mode at BM25-SpLine at the European Synchrotron Radiation Facility (ESRF) in Grenoble (France). For each sample and edge, at least 4 or 5 scans were acquired and merged in order to increase the signal to noise ratio. The spectra were acquired upon wavenumber values of 15 $Å^{-1}$. To obtain the Fourier transform (FT) of the extended XAFS (EXAFS) and to perform the corresponding fits in the real and photoelectron wave vector (k) space, a k range from 2.5 to 14 $Å^{-1}$ was analyzed for all spectra. Branch A of the BM25 beamline is equipped with a double Si(111) crystal monochromator of pseudo–channel cut type, refrigerated at 200 K by an ethanol cooling system. The fluorescence detector is an energy-dispersive 13-element Si(Li) multidetector from SGX Sensortech. An Fe foil was used to calibrate the energy. EXAFS data were reduced applying standard procedures using the Demeter package [22], and fits on k^3-weighted signals were carried out in r and k space using theoretical functions from FEFF8.4 code [23]. In the fitting procedure, the number of atoms for each atomic path or coordination number has been set to the nominal value of the FEFF calculation. This means 8 for the first atomic shell, 6 for the second, and 12 for the third. Within the fitting of a group of measurements, the nonstructural parameter, the energy shift (ΔE_0), was set free for convergence reasons but strongly constrained to an interval of ± 1 eV with respect to the value obtained for the first fitting of each series. For the x-ray absorption near edge structure (XANES), the software package FDMNES [24] was employed to perform the full multiple scattering calculations on the Ga K edge. Crystallographic files for the orthorhombic Ga [25] and a modified bcc Fe crystallographic datasheet [25] were employed for the first calculations, which were eventually modified to suit the current systems for calculating the $A2$ and the $D0_3/B2$ structures. The software CRYSTALFFREV [26] was employed to create the FEFF input files, including those from structures with partial occupation.

III. EXPERIMENTAL RESULTS AND DISCUSSION

To know the flow regime for each L, it is necessary to calculate λ. Following Álvarez *et al.* [18], we use the expression

$$\lambda = \frac{1}{\frac{\sigma_g}{\nu k_B T_g} \cdot p_g} \tag{1}$$

where σ_g is the cross section for an elastic scattering event between a neutral and a plasma gas atom, k_B is the Boltzmann constant, T_g is the plasma temperature, ν is the number of subsequent elastic collisions required for the thermalization of the neutrals, and p_g is the gas pressure.

We calculate σ_g for Fe($\sigma_{g,\mathrm{Fe}}$) and Ga($\sigma_{g,\mathrm{Ga}}$) considering their atomic radius and atomic masses as also proposed by R. Álvarez and coworkers [18].

$$\sigma_{g,\mathrm{Fe}} = \pi (R_{\mathrm{Fe}} + R_{\mathrm{Ar}})^2 \sqrt{1 + \left(\frac{M_{\mathrm{Fe}}}{M_{\mathrm{Ar}}}\right)} = 2.2 \times 10^{-19}\ \mathrm{m}^2 \tag{2}$$

$$\sigma_{g,\mathrm{Ga}} = \pi (R_{\mathrm{Ga}} + R_{\mathrm{Ar}})^2 \sqrt{1 + \left(\frac{M_{\mathrm{Ga}}}{M_{\mathrm{Ar}}}\right)} = 2.1 \times 10^{-19}\ \mathrm{m}^2 \tag{3}$$

We take $\nu = 2$ for both Fe and Ga. Álvarez *et al.* [18] considered a T_g of 400 K for sputtering deposition at room temperature with a growth power of 300 W. Taking into account that we used lower growth powers and lower T_g values than other authors report [27], we estimated 325 K for T_g. Introducing p_g, σ_g, T_g, and ν in Eq. (1), we obtain a λ of around 14 cm for the two atomic species Fe and Ga. Then, for $L = 9$ cm, the neutrals move from the target to the substrate with ballistic flow, whereas it is diffusive for $L = 14$ cm.

In Fig. 1 we compare the XRD patterns of layers deposited with the same growth power in the ballistic and in the diffusive flow. In both cases, the main diffraction peak is related to the (110) reflection of the α-Fe structure as generally observed in Fe-Ga thin films [11,15]. The two samples also show a rather small diffraction peak corresponding to Fe(211). The absence of both a diffraction peak at $2\theta \sim 30.7°$ related to the (100) reflection and a peak splitting around the (220) reflection at $2\theta \sim 97°$ rules out the presence of $D0_3$ clusters with a size equal to or greater than 100 nm [9]. Although bulk samples with a similar Ga content are mainly formed by the ordered $D0_3$ phase, previous papers on Fe-Ga thin films report that the disordered $A2$ phase is kept for a Ga content of 30 at.% [6]. From the angular position of the (110) peak and considering the bcc structure of the samples [Fig. 1(b)], we can infer the lattice parameter. Assuming that the variations on the angular position are only due to compositional differences, we obtain a lattice parameter of 2.8949 (8) Å for the diffusive and 2.8934 (8) Å for the ballistic layer, respectively. The slightly higher lattice parameter of the sample deposited at $L = 14$ cm can be correlated with a higher Ga content in that sample. We measured by means of EDS the composition of the samples. In agreement with the tendency observed in the XRD results, we detect a higher Ga content, ~32 at.%, for the sample deposited in the diffusive regime compared with the ~28 at.% Ga measured in the ballistic regime. When neutrals arrive thermalized at the growing surface ($L = 14$ cm), the probability of being introduced in the lattice is higher for

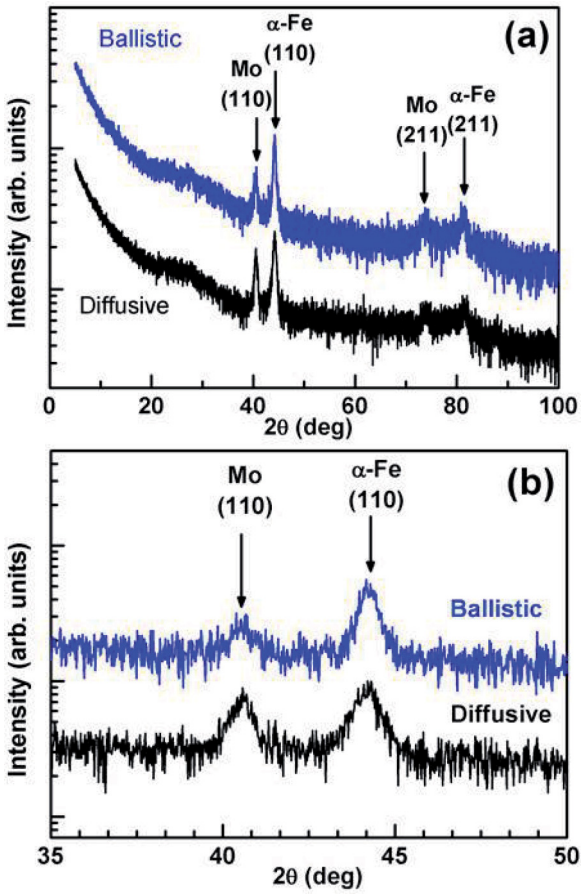

FIG. 1. X-ray diffraction patterns in the Bragg–Brentano configuration for the Fe-Ga films deposited at a distance of 9 cm (ballistic regime) and 14 cm (diffusive regime). (a) The complete diffractograms and (b) a detail of the curves around the (110) diffraction peak of the α-Fe structure. The curves are vertically shifted for clarity.

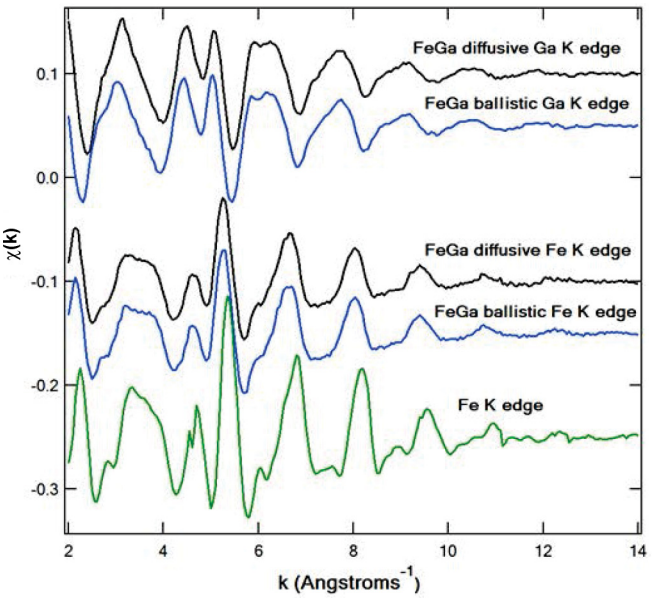

FIG. 2. Normalized EXAFS spectra as a function of the photoelectron wave vector k of the Fe and Ga K edges. Top curves: oscillations at the Ga K edge of the ballistic and diffusive samples; middle curves: corresponding spectra at the Fe K edge; bottom curves: spectrum of the bulk Fe reference.

lower surface energies. The higher Ga content observed in the diffusive sample can be explained by the lower surface energy of Ga (2.78 eV) compared with Fe (4.29 eV) [28]. If we compare the lattice parameter of our samples with reported values for sputtered layers with an equivalent Ga content [11], we find reasonable values considering the rather wide range of reported parameters. We calculated the ratio between the intensity of the Fe(110) and Mo(110) diffraction peaks ($I_{Fe(110)}/I_{Mo(110)}$). The higher value obtained for the ballistic layer, $I_{Fe(110)}/I_{Mo(110)} = 1.7$, compared with the diffusive, $I_{Fe(110)}/I_{Mo(110)} = 1.1$, indicates a higher (110) texture in the ballistic case. The Fe(110) diffraction peak is taken to estimate the crystallite size by means of the Scherrer equation in both cases. The larger crystallite size obtained for the ballistic (D = 14.0 nm) compared with the diffusive sample (D = 11.2 nm) points to a higher long-range structural order in the former case.

In the ballistic regime, the neutrals retain at their arrival at the growing surface the energy and momentum gained when they were ejected from the target. However, in the diffusive flow, the neutrals arrive thermalized and with a random orientation at the substrate. XRD has not demonstrated to be a decisive technique to detect the $D0_3$ and $B2$ phases in Fe-Ga alloys with a Ga content of about 25 at.% [29], and our XRD measurements are not conclusive to detect traces of these phases because of experimental sensitivity. Thus, we performed EXAFS in two representative samples deposited in the ballistic and diffusive regimes to analyze the influence of the flow regime on the local atomic order. Furthermore, XAFS, as previously employed by other authors to study Fe-Ga alloys with Ga content of 20 at.%, has proved to be a very useful tool in these kinds of systems [30]. The EXAFS spectra reduced from the XAFS raw data are presented in Fig. 2 as a function of k. In this figure, the spectra at the Fe and Ga K edges are shown, as well as the corresponding spectra of the Fe foil acquired under the same conditions. In Fig. 3, we present the FT of the EXAFS spectra for the Fe K edge of the aforementioned samples in the k range from 2.5 to 14 Å^{-1}. In order to get information about the local structure, we fitted the first three atomic shells of the EXAFS spectra. In our model, we placed uniformly distributed Ga atoms, in accordance with the average Ga concentration, in a metallic Fe reference to get the paths for the calculations. The calculated EXAFS parameters for the local structure of Fe corresponding to the two studied systems are summarized in Table I and compared with a bulk metallic Fe reference (the Fe foil).

The results show that the radial distance of the shells of both sputtered samples increases with respect to the bulk Fe reference, as already pointed out by XRD. This can be explained by the mean bonding distance increase due to the inclusion of Ga in the Fe lattice. More clues about the local structure of Fe in the alloys can be found regarding the variance of the expected radial distance of each shell (Debye–Waller [DW] factor) which accounts for the correlative disorder between the scattered atom and the atoms existing in their

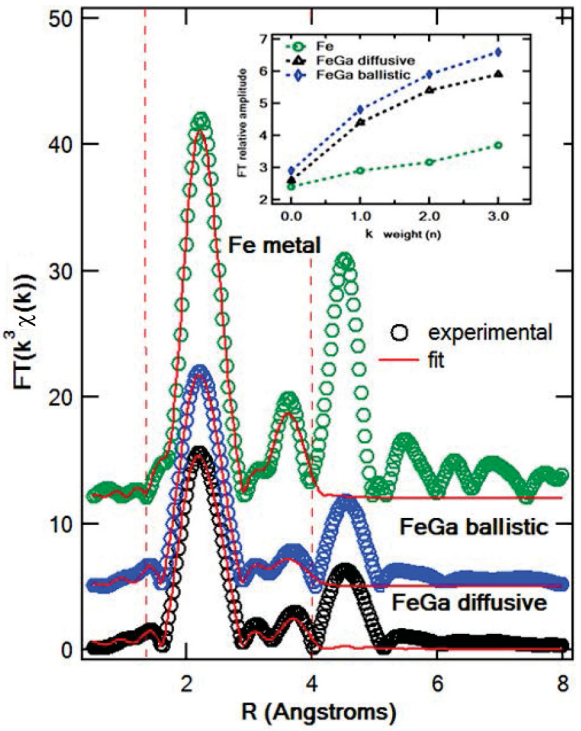

FIG. 3. FT EXAFS spectra and corresponding fittings at the Fe K edge of the Fe-Ga layers grown in the ballistic and the diffusive regime and of the bulk Fe reference. Inset: FT amplitude as a function of the wave-number weight for the EXAFS spectra.

respective shells. In this case, we can observe values relatively higher (∼50%) than those corresponding to the bulk Fe reference (Table I). In the case of the ballistic sample, the DW factor of the first atomic shell is noticeably lower than for the diffusive sample in all the fitted atomic shells (Table I). Hence, for both samples, the DW values deviate for higher order shells, evidencing a more disordered, less long term correlative order, which can be attributed to the random presence of Ga in the lattice distorting the original Fe structure. For the diffusive layer, the calculated values are larger than for the ballistic (on average, ∼15% larger), which indicates a lower local atomic order in the diffusive sample (Table I). The differences vanish for the furthest shell included in the model, where both converge to similar values of disorder.

TABLE I. EXAFS parameters obtained from the fit of the Fe K edge spectra of the Fe-Ga samples obtained by diffusive and ballistic regimes as well as the parameters for the bulk Fe reference.

	Diffusive	Ballistic	Fe
R Fe-Fe1 (Å)	2.500 (1)	2.498 (2)	2.474 (2)
R Fe-Fe2 (Å)	2.887 (1)	2.885 (2)	2.870 (2)
R Fe-Fe3 (Å)	4.082 (2)	4.080 (3)	4.045 (3)
DW-fFe-Fe1(σ^2)(Å^2)	0.0093 (7)	0.0082 (4)	0.0056 (5)
DW-fFe-Fe2(σ^2) (Å^2)	0.0154 (10)	0.0111 (10)	0.0055 (8)
DW-fFe-Fe3(σ^2) (Å^2)	0.0230 (4)	0.0200 (4)	0.0093 (15)
ΔE_0(eV)	4.0 (5)	4.5 (6)	4.5 (5)
R coefficient	0.010	0.011	0.006

TABLE II. EXAFS parameters obtained from the fit of the Ga K edge spectra of the Fe-Ga samples obtained by diffusive and ballistic regimes.

	Diffusive	Ballistic
R Ga-Ga1 (Å)	2.570 (2)	2.566 (2)
R Ga-Ga2 (Å)	2.967 (2)	2.963 (2)
R Ga-Ga3 (Å)	4.197 (2)	4.191 (3)
DW-Ga-Ga1(σ^2) (Å^2)	0.0078 (7)	0.0077 (4)
DW-Ga-Ga2(σ^2) (Å^2)	0.039 (10)	0.021 (10)
DW-Ga-Ga3(σ^2) (Å^2)	0.017 (4)	0.015 (4)
ΔE_0 (eV)	–3 (2)	–4 (2)
R coefficient	0.018	0.014

As already mentioned, we made the calculations by considering a mix of both Ga and Fe in the path file construction. The effect of Ga insertion in the initial Fe lattice did not considerably modify the path intensities. Nevertheless, we also evaluated the impact of the Ga inclusion in the Fe local structure of the Fe-Ga samples by comparing the FT of the EXAFS weighted for different powers of k, namely k^0, k^1, k^2, and k^3. Measuring the relative intensity of the first and second more intense peaks of the FT in r space at different k weights can be used to estimate the atomic number (Z) of the atoms in the surroundings of the scattered atom [22]. As Ga is an element with larger Z, the amplitude of the FT at the corresponding shell should diverge more rapidly for increasing k weights than for Fe. The inset of Fig. 3 shows the evolution of the relative intensity of the first peak to the second one in the FT for the samples and for the bulk Fe. The peak ratio for the Fe-Ga layers clearly diverges compared with bulk Fe from the zero to the third order.

The Ga K edge gives more information about the particularities of each system. To model the Ga local structure, we considered a bcc structure occupying the Fe sites in the lattice. The fitting parameters are summarized in Table II and the best fits obtained for the r space are shown in Fig. 4. Following the order of parameters for the Ga K edge (Table II), we tried to match them with the results for the Fe K edge (Table I). Differences in the mean shell distances are observed between samples. The Ga-Ga/Fe mean distance in the diffusive sample is slightly larger than for the ballistic case. This difference is within experimental accuracy, but it may be regarded as a tendency, and more information can be obtained by analyzing the DW factors of the first shells. Attending to the local correlative order between shells, values very close to those obtained for the Fe K edge are observed for the first shell. Nevertheless, for the second atomic shell, this disorder is noticeably larger and rapidly increases with distance. The additional disorder, especially at orders over first, is considerably higher for the diffusive sample and will be discussed below. The interatomic distances between shells are also noticeably dilated compared with the Fe bcc structure. This is partially expected due to the larger Ga ionic radii but can also be an indication of the nature of the mean first neighbors of Ga. In this sense, we can make a qualitative estimation of the type of atoms that mainly surround Ga similar to that performed for the Fe K edge. We obtain the k weight

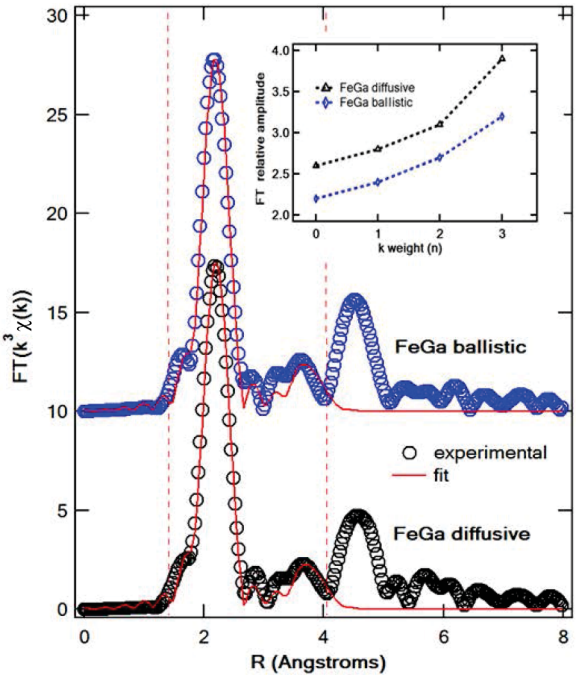

FIG. 4. FT EXAFS spectra and corresponding fittings at the Ga K edge of the Fe-Ga layers grown in the ballistic and diffusive regimes. Inset: FT amplitude dependence as a function of the wave number weight for the EXAFS spectra displayed.

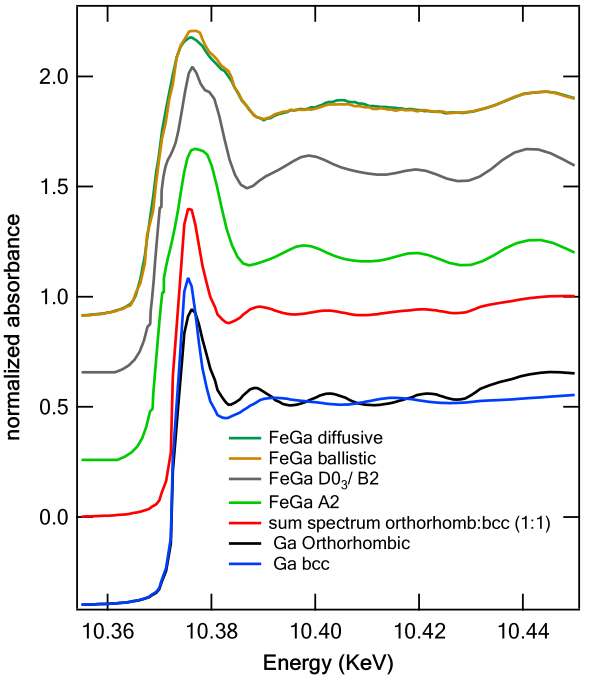

FIG. 5. XANES experimental spectra at the Ga K edge of the Fe-Ga samples obtained in the diffusive and ballistic regimes and the theoretical XANES spectra for bcc and orthorhombic Ga phases and a combined spectrum considering a 1:1 contribution of the bcc:orthorhombic phases, as well as the calculated Ga K edge XANES spectra of the $B2$ and $A2$ structures.

dependence of the FT intensity in both samples (Fig. 4 inset). We can appreciate that both curves straightly follow a parallel tendency, with a slight divergence in the diffusive sample for the highest k evaluated values. This can be taken as an indication of the highest amount of Ga in the surroundings (few first angstroms from the photoelectron origin) for the diffusive layer.

In this sense, it is also worth observing the XANES region of the Ga K edge absorption spectra for both samples (Fig. 5). Subtle but clear differences can be envisaged in the shape and intensity of the white line (the region just after the edge jump) and in the second resonance after the edge. The XANES region of the XAS is highly sensitive to changes in the local geometry (in general, by "local" we refer to volumes within a radius of few angstroms), symmetry, and atomic coordination and also to slight changes in the electronic structure. The corresponding XANES for the Fe K edge did not show any differences for both samples, so it seems that the observed changes mainly happen in the Ga local structure. Considering the higher sensitivity of the Ga K edge to the particularities of the studied alloys compared with that of Fe observed in our samples, we performed full multiple scattering calculations in order to simulate the experimental XANES spectra of Ga. We simulated different Ga structures, including Ga in a bcc structure, Fe-Ga in the $A2$ and $D0_3/B2$ order, and Ga in its most natural solid state structure, the orthorhombic. We consider the $D0_3/B2$ order indistinguishable since, from the point of view of XAFS, which is only sensitive to local structure, $D0_3$ is equivalent to $B2$ and cannot be differentiated. In this regard, one can consider a $D0_3$ order as a superstructure of the $B2$, which can be identified by XRD but not by XAFS. Thus, when discussing XANES data hereafter, we will refer to the $D0_3/B2$ order as completely equivalent from the XAFS point of view.

Results of the XANES calculations are presented in Fig. 5 with the experimental spectra of the Ga for both ballistic and diffusive deposition conditions. The $A2$ and $D0_3/B2$ theoretical spectra present clear differences in the white line and in the multiple structure resonances after the absorption peak. Compared with the experimental spectra, the calculated main edge peak is considerably narrower in the case of the bcc and orthorhombic Ga. As previously studied by Farges *et al.* [31], the broadening of the experimental peak can be interpreted as an indication of short- to medium-range disorder. The disorder makes the absorption sites (Ga atoms in this case) to be less localized on average, with a wider spatial distribution and variation in E_0 (energy of the absorption edge). As a second consequence, this disorder can induce a damping in the EXAFS magnitude because of higher terms in the DW expansion (cumulant expansion coefficients of third and fourth order). One effect, the delocalization of absorption sites, is considered here to have an appreciable effect in the XANES spectra. The main $A2$ phase implies a randomly distribution of Ga in the unit cell of the bcc structure, and it is naturally more disordered. As a consequence, it yields to a broader and less defined edge shape. As can be appreciated in Fig. 5, this effect is reflected by a clear broadening of the main peak and the appearance of a shoulder at lower energies that is related to a symmetry reduction of the Ga environment. In the $D0_3/B2$ phase, this shoulder is also

observed, and the main peak is resolved in two differentiated structures that resemble the spectrum shape of the ballistic sample. For the diffusive sample, the shape at energies just after the main peak is not so clearly resolved. The features of the ballistic layer at energies near the edge, then, may indicate a higher amount of a more ordered $D0_3/B2$ phase in the ballistic compared with the diffusive layer. In the experimental and simulated Fe-Ga ($A2$ and $D0_3/B2$), as well as in the orthorhombic Ga spectra, another feature is observed at 10.44 keV that may also be related to a symmetry breaking of the Ga environment (not observed in the pure bcc Ga). The spectra of both samples also exhibit a small feature at 10.405 keV, much more prominently in the diffusive layer, which coincides with none of the theoretical bcc spectra but does with that observed in the orthorhombic Ga theoretical spectra at the same energy position. This last aspect can be associated with the higher shell-to-shell correlated disorder obtained from the EXAFS model employed, which uses a bcc structure as its basis. The higher content of a nonpure bcc phase and the coexistence of different bcc subphases should push the variance of the atomic shell position (DW factor) to higher values, as has been obtained in the calculations, especially for the diffusive sample. If all these aspects are taken into account, the coexistence of both phases, bcc and orthorhombic, can induce peak broadening and disappearance of the shoulder at lower energies, especially those observed in the diffusive layer. Thus, the features of this sample can be a combination of the existence of both a more prominent presence of a disordered $A2$ phase with respect to the ordered $D0_3/B2$ phases and of orthorhombic Ga clusters. A number of papers studied Fe-Ga thin films [6,11–17,32–34] and, more specifically, deposition by sputtering [11–17], although few papers explore thin films with the composition range studied in this paper [6,11,35]. The paper by Dunlap *et al.* [11], in which they studied sputtered Fe-Ga alloys with a (110) texture, is the most similar to the current case. More interestingly, in that paper they already start to find indications of Ga clusters for Ga $\sim$ 28 at.% for Ga content above the stoichiometric composition for the ordered $D0_3$ phase (Ga $>$ 25 at.%), which is in agreement with the present paper. However, they did not give any further information about the structure of these clusters. Our experimental results indicate that the nature of such aggregates could be, at least partially, orthorhombic Ga.

XRD and EDS coincide and provide information about the composition of layers of 32 at.% Ga for the diffusive and 28 at.% Ga for the ballistic. In the diffusive layer, we found by XRD a lower long-range structural quality, indicated by both the smaller crystallite size and (110) texture. XAFS has provided element-selective, local insight into disordered regions, including phases not detectable by XRD. In the diffusive layer, the combination of EXAFS and XANES has been used to detect a higher presence of the disordered $A2$ phase and evidence of Ga clusters. On the other hand, the experimental results suggest a higher proportion of ordered $D0_3/B2$ phases in the ballistic layer. Thus, the local and long-range structural characterization techniques indicated a more disordered system in the diffusive layer. The sensitivity of XAFS for disordered atomic arrangements is crucial to understand EDS and XRD results altogether. If we consider

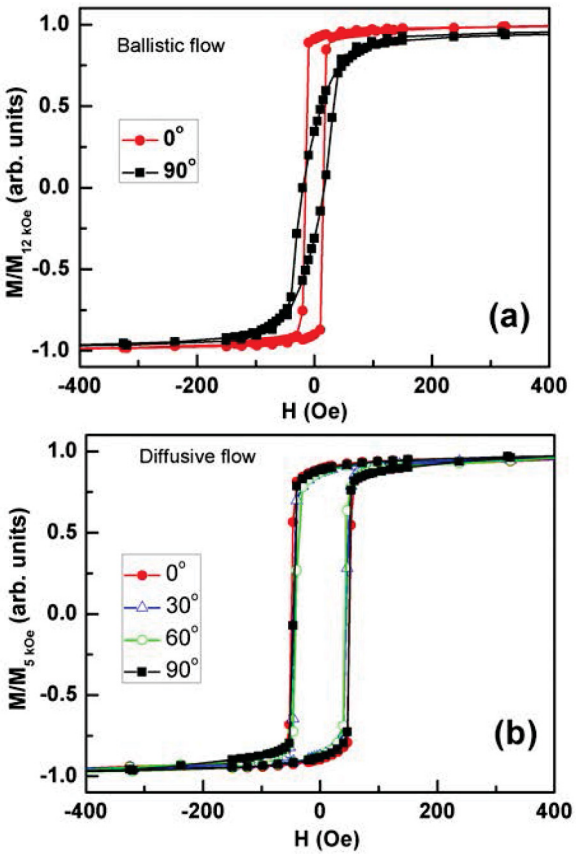

FIG. 6. (a) Hysteresis loops measured at room temperature for an Fe-Ga layer deposited in the ballistic flow. The loops were measured at different angles between a reference direction and the in-plane magnetic field: (•) 0° and (■) 90°. (b) Hysteresis loops measured at room temperature for an Fe-Ga layer deposited in the diffusive flow. The loops were measured at different angles between a reference direction and the in-plane magnetic field: (•) 0°, (△) 30°, (○) 60°, and (■) 90°.

a higher presence of the disordered $A2$ phase in the diffusive sample, which also has a higher Ga content, it can also explain the increase in disorder for the Fe local structure. The different proportion of Ga content in the studied samples appears to be due to the flow regime. We cannot rule out that the small compositional variations between the diffusive (Ga $\sim$ 32 at.%) and the ballistic (Ga $\sim$ 28 at.%) layers are the sole cause of the observed differences in their structure, but it is important to remark that we obtained different compositions and clear structural differences (local and long range) upon the use of different flow regimes.

We performed a study on the effect of the growth regime on the global magnetic properties of the Fe-Ga layers. In Figs. 6(a) and 6(b) we present the in-plane hysteresis loops measured at room temperature for the layers analyzed by XAFS. To study the in-plane magnetic behavior, the magnetic field has been applied, forming different angles with respect to a reference direction taken as the intersection between the incidence and the substrate planes [36]. The ballistic layer exhibits a magnetic easy axis in the reference direction [Fig. 6(a)], in agreement with previous papers about other magnetic systems also deposited in oblique incidence [36–38].

However, the layer deposited under diffusive flow has isotropic behavior [Fig. 6(b)]. While the magnetic anisotropy of pure Fe is 4.8×10^4 J m^{-3}, we obtained a value of 2.1×10^4 J m^{-3} for the ballistic layer and a residual value of 1.1×10^4 J m^{-3} for the diffusive layer. The magnetic anisotropy obtained in the ballistic case is similar to the value reported in sputtered layers [12], whereas the diffusive layer exhibits a lower value. Therefore, the different structure promoted by each flow regime has an impact on the magnetic properties of these compounds. We cannot use the model proposed by Cullen *et al.* [10] because it is only valid when Ga concentration is within the range 0–20 at.%. It seems that the lower structural order of the diffusive layer is the origin of its in-plane magnetic isotropy. Inhomogeneities such as the existence of multiple phases and imperfections in the crystal can lead to local fluctuations of the magnetization, which in turn reduce the magnetic anisotropy [39]. In the diffusive layer we obtained indications of a higher proportion of a disordered $A2$ phase and Ga-rich aggregates, as well as smaller crystallite size and lower (110) texture. This higher number of inhomogeneities and associated defects might promote the loss of in-plane magnetic anisotropy. However, the ballistic layer has a more ordered structure, as indicated by XRD (higher texture and larger crystallites), with Ga more homogeneously introduced in the Fe matrix, with the proportion of $A2$ phase smaller, as observed by EXAFS and XANES. These structural properties seem to enable a $K_{\text{in-plane}}$ similar to other reported values [12]. This is a first approximation to the experimental results and a more detail model must be performed to explain the correlation between structural properties and magnetic anisotropy around the second peak of magnetostriction to provide a complete description of the results.

IV. CONCLUSIONS

We investigated the influence of flow regime on the structural properties of Fe-Ga thin films deposited by sputtering. We explored the composition range around the second peak of magnetostriction for these compounds (Ga $\sim$ 30 at.%). The diffusive flow promotes a higher amount of Ga, and the experimental results point to a more prominent presence of the $A2$ phase, with a more disordered structure due to the randomly distributed Ga in the bcc structure, and to a higher proportion of orthorhombic Ga clusters. A higher structural order is observed in the ballistic layer, with a more probable presence of the ordered $D0_3/B2$ phases. XRD has also indicated a higher long-range structural quality in the ballistic sample (larger texture and crystallite size). All these differences seem to affect the magnetic behavior of the layers. While we obtain a clear in-plane magnetic anisotropy in the layer deposited in the ballistic regime, the diffusive sample shows isotropic behavior. Therefore, results indicate that flow regime can be used to control the magnetic anisotropy of Fe-Ga thin films with a Ga content of around 30 at.%.

ACKNOWLEDGMENTS

This paper has been financially supported through of the Spanish Ministry of Economy and Competitiveness (MINECO), MAT2015-66888-C3-3-R. We thank "CAI Difracción de rayos-X" of Universidad Complutense de Madrid for the x-ray diffractometry measurements and Instituto de Sistemas Optoelectrónicos y Microtecnología (ISOM) for the use of some of its facilities. We also thank BM25-SpLine, the Spanish CRG at ESRF for providing beam time.

[1] A. E. Clark, J. B. Restorff, M. Wun-Fogle, T. A. Lograsso, and D. L. Schlagel, IEEE Trans. Magn. **36**, 3238 (2000).
[2] A. E. Clark, M. Wun-fogle, T. A. Lograsso, and J. R. Cullen, IEEE Trans. Magn. **37**, 2678 (2001).
[3] M. Laver, C. Mudivarthi, J. R. Cullen, A. B. Flatau, W.-C. Chen, S. M. Watson, and M. Wuttig, Phys. Rev. Lett. **105**, 027202 (2010).
[4] M. P. Ruffoni, S. Pascarelli, R. Grossinger, R. S. Turtelli, C. Bormio-Nunes, and R. F. Pettifer, Phys. Rev. Lett. **101**, 147202 (2008).
[5] H. Cao, P. M. Gehring, C. P. Devreugd, J. A. Rodriguez-Rivera, J. Li, and D. Viehland, Phys. Rev. Lett. **102**, 127201 (2009).
[6] E. Arenholz, G. van der Laan, A. McClure, and Y. Idzerda, Phys. Rev. B **82**, 180405 (2010).
[7] O. Ikeda, R. Kainuma, I. Ohnuma, K. Fukamichi, and K. Ishida, J. Alloys Compnd. **347**, 198 (2002).
[8] Q. Xing, Y. Du, R. J. McQueeney, and T. A. Lograsso, Acta Materialia **56**, 4536 (2008).
[9] H. Cao, F. Bai, J. Li, D. Viehland, T. A. Lograsso, and P. M. Gehring, J. Alloys Compnd. **465**, 244 (2008).
[10] J. Cullen, P. Zhao, and M. Wuttig, J. Appl. Phys. **101**, 123922 (2007).
[11] R. A. Dunlap, N. C. Deschamps, R. E. Mar, and S. P. Farrell, J. Phys.: Condens. Matter **18**, 4907 (2006).
[12] A. Butera, J. Gómez, J. L. Weston, and J. A. Barnard, J. Appl. Phys. **98**, 033901 (2005).
[13] R. R. Basantkumar, B. J. Hills Stadler, W. P. Robbins, and E. M. Summers, IEEE Trans. Magn. **42**, 3102 (2006).
[14] J. L. Weston, A. Butera, T. Lograsso, M. Shamsuzzoha, I. Zana, G. Zangari, and J. Barnard, IEEE Trans. Magn. **38**, 2832 (2002).
[15] B. Adolphi, J. McCord, M. Bertram, C.-G. Oertel, U. Merkel, U. Marschner, R. Schäfer, C. Wenzel, and W.-J. Fischer, Smart Mater. Struct. **19**, 055013 (2010).
[16] B. W. Wang, S. Y. Li, Y. Zhou, W. M. Huang, and S. Y. Cao, J. Magn. Magn. Mater. **320**, 769 (2008).
[17] Y. Zhang, Q. Zhan, Z. Zuo, H. Yang, X. Zhang, G. Dai, Y. Liu, Y. Yu, J. Wang, B. Wang, and R. W. Li, Phys. Rev. B **91**, 174411 (2015).
[18] R. Álvarez, J. M. García-Martín, M. C. Lopez-Santos, V. Rico, F. J. Ferrer, J. Cotrino, A. R. González-Elipe, and A. Palmero, Plasma Process. Polym. **11**, 571 (2014).
[19] R. E. Somekh, J. Vac. Sci. Technol. A **2**, 1285 (1984).
[20] G. M. Turner, I. S. Falconer, B. W. James, and D. R. McKenzie, J. Vac. Sci. Technol. A **10**, 455 (1992).
[21] C. V. R. Vasant Kumar and A. Mansingh, J. Appl. Phys. **65**, 1270 (1989).
[22] B. Ravel and M. Newville, J. Synchrotron Rad. **12**, 537 (2005).
[23] A. L. Ankudinov, B. Ravel, J. J. Rehr, and S. D. Conradson, Phys. Rev. B **58**, 7565 (1998).
[24] Y. Joly, Phys. Rev. B **63**, 125120 (2001).
[25] R. W. G. Wyckoff, in *Crystal Structures*, 2nd ed. (Interscience Publishers, New York, 1963), Vol. 1, pp. 7–83.

[26] M. Alain, M. Jacques, M.-B. Diane, and P. Karine, J. Phys.: Conf. Ser. **190**, 012034 (2009).
[27] C. H. Shon and J. K. Lee, Appl. Surface Science **192**, 258 (2008).
[28] Donald H. Buckley, *Surface Effects in Adhesion, Friction, Wear, and Lubrication* (Elsevier, Amsterdam, 1981).
[29] J. M. Borrego, J. S. Blázquez, C. F. Conde, A. Conde, and S. Roth, Intermetallics **15**, 193 (2007).
[30] S. Pascarelli, M. P. Ruffoni, R. Sato Turtelli, F. Kubel, and R. Grössinger, Phys. Rev. B **77**, 184406 (2008).
[31] F. Farges, G. E. Brown, and J. J. Rehr, Phys Rev B **56**, 1809 (1997).
[32] R. Ranchal and D. Maestre, J. Phys. D: Appl. Phys. **47**, 355004 (2014).
[33] S. Tacchi, S. Fin, G. Carlotti, G. Gubbiotti, M. Madami, M. Barturen, M. Marangolo, M. Eddrief, D. Bisero, A. Rettori, and M. G. Pini, Phys. Rev. B **89**, 024411 (2014).
[34] S. Fin, R. Tomasello, D. Bisero, M. Marangolo, M. Sacchi, H. Popescu, M. Eddrief, C. Hepburn, G. Finocchio, M. Carpentieri, A. Rettori, M. G. Pini, and S. Tacchi, Phys. Rev. B **92**, 224411 (2015).
[35] M. Barturen, B. Rache Salles, P. Schio, J. Milano, A. Butera, S. Bustingorry, C. Ramos, A. J. A de Oliveira, M. Eddrief, E. Lacaze, F. Gendron, V. H. Etgens, and M. Marangolo, Appl. Phys. Lett. **101**, 092404 (2012).
[36] M. Maicas, R. Ranchal, C. Aroca, P. Sánchez, and E. López, Eur. Phys. J. B **62**, 267 (2008).
[37] K. Hara, T. Hashimoto, and E. Tatsumoto, J. Phys. Soc. Jpn. **28**, 254 (1970).
[38] R. E. Jones, J. Williams, L. Spector, C.-J. Lin, S. Wang, S. Pichai, and B. M. Clemens, IEEE Trans. Magn. **31**, 3817 (1995).
[39] J. Atulasimha, A. B. Flatau, and J. R. Cullen, Smart Mater. **17**, 025027 (2008).